SYNTHESIS OF GRAPHENE/Mn$_{0.2}$Cd$_{0.8}$S HIERARCHICAL NANOSPHERES FOR PHOTOCATALYTIC DEGRADATION OF ORGANIC POLLUTANTS

B. ZENG[a,b], R. WANG[b,*]
^{a}College of Mechanical Engineering, Hunan University of Arts and Science, Changde 415000, People's Republic of China
^{b}Hunan Collaborative innovation Center for construction and development of Dongting Lake Ecological Economic Zone, Changde 415000, People's Republic of China

The hierarchically structured hybrids of graphene and Mn$_{0.2}$Cd$_{0.8}$S solid-solution, resulting in G/Mn$_{0.2}$Cd$_{0.8}$S HN, are successfully synthesized by using microwave method with the assistance of L-Histidine. Moreover, X-ray diffraction (XRD), UV-vis absorption spectroscopy, scanning electron microscopy (SEM) and transmission electron microscopy (TEM) are employed to analyze the structural and optical properties. Furthermore, the decoloration of methyl orange (MO) under visible light irradiation indicates that the G/Mn$_{0.2}$Cd$_{0.8}$S HN is a promising photocatalyst for the degradation of organic pollutants. Herein, a possible photocatalytic mechanism of G/Mn$_{0.2}$Cd$_{0.8}$S is proposed, showing the synergistic influence of hierarchical nanospheres morphology, optimal bandgap and conductive graphene scaffold on photocatalytic activity. Overall, the photodegradation performance is improved due to the effective separation of electron/hole pairs and efficient transportation of photogenerated electrons from Mn$_{0.2}$Cd$_{0.8}$S to graphene. The current work demonstrates an environment-friendly route to fabricate multi-component chalcogenides for high-performance photocatalytic applications.

1. Introduction

Semiconducting photocatalysts render great potential in solving environmental pollution and meeting clean energy requirements[1]. Sulfide-based metal materials are promising for a wide range of applications due to narrow bandgap and suitable conduction edge[2]. In particular, Cadmium sulfide (CdS) has been extensively investigated as a photocatalyst for water treatment application. In addition to the narrow bandgap, an ideal photocatalyst should exhibit effective charge carrier separation[3]. Thus, different approaches have been adopted to tune the bandgap and enhance the charge separation of CdS, such as preparation of solid-solutions and carbon/CdS hybrids[4]. By choosing the proper components, cadmium sulfide solid solution can form the suitable band structure. For instance, a large variety of multi-component CdS-based solid-solutions, such as Mn$_{1-x}$Cd$_x$S, Zn$_x$Cd$_{1-x}$ and Cd$_x$Pb$_{1-x}$S, have been synthesized, showing excellent control over bandgap and superior charge separation behavior[5-6]. In particular, ternary Mn$_{1-x}$Cd$_x$S solid-solution, which is formed by the consolidation of CdS (2.4 eV) and MnS (3.7 eV), renders a band-gap with the deep negative conduction band (CB) edge[7].

However, a single-component solid-solution renders low charge-separation efficiency. On the other hand, hierarchical nanospheres efficiently separate charge carriers by decreasing the transportation distance of the charges from the inside to the surface[8-9]. Hence, hierarchical Mn$_{1-x}$Cd$_x$S nanospheres are expected to exhibit better photocatalytic performance than CdS nanoparticles.

Moreover, the photocatalytic efficiency can be further improved by coupling Mn$_{1-x}$Cd$_x$S solid-solution with graphene, where the graphene provides high surface area for anchoring of

---

catalytic particles and reduces recombination loss by separating photoinduced electrons and holes. However, the synthesis and photocatalytic properties of $Mn_{1-x}Cd_xS$/graphene hybrids have not been reported yet.

Herein, we report the synthesis of highly-efficient graphene/$Mn_{0.2}Cd_{0.8}S$ hierarchical nanospheres (G/$Mn_{0.2}Cd_{0.8}S$ HN) by using an environment-friendly biomolecule-assisted method. Moreover, the photocatalytic behavior of G/$Mn_{0.2}Cd_{0.8}S$ HN is evaluated under visible light irradiation and the photocatalytic mechanism is discussed in detail.

2. Experimental details

2.1. Preparation of graphene/$Mn_{0.2}Cd_{0.8}S$ hierarchical nanospheres

The G/$Mn_{0.2}Cd_{0.8}S$ HN samples were prepared by the microwave-assisted hydrothermal method. In a typical process, 0.005 g of graphene oxide, 1 mmol of manganese (II) acetate tetrahydrate ($Mn(AC)_2.4H_2O$, $\geqslant$ 99.99% purity, Aladdin), 4 mmol of cadmium acetate dihydrate ($Cd(AC)_2.2H_2O$, $\geqslant$ 99.99% purity, Aladdin), 1 g of L-Histidine and 5 mmol of thioacetamide (C_2H_5NS, $\geqslant$ 99.0% purity, Aladdin) were sequentially added into 80 mL deionized water. After stirring for 30 min, the solution was transferred into a microwave chemical reactor (MCR-3) and heated at 200 ℃ for 30 min. The grey precipitate was recovered by filtration, washed with an aqueous solution five times and dried at 80 ℃ for 1 h. For comparison, CdS hierarchical nanospheres (CdS HN) were prepared by the same method without adding graphene oxide and $Mn(AC)_2.4H_2O$ in the solution, where the G/CdS hierarchical nanospheres (G/CdS HN) were obtained by excluding $Mn(AC)_2.4H_2O$ precursor.

2.2. Material characterization

Powder X-ray diffraction (XRD) was performed by using a Siemens D5000 diffractometer, equipped with Cu Kα radiations. The morphology and microstructure were characterized by scanning electron microscope (SEM, Hitachi S-4800) and transmission electron microscopy (TEM, JEOL JEM-2100F), equipped with energy dispersive X-ray spectrometer (EDS, JEOL JEM-2100F). X-ray photoelectron spectroscopy (XPS) was carried out by using a K-Alpha 1063 spectrometer, equipped with Al Kα radiations.

2.3. Photocatalytic characterization

The photocatalytic performance of methyl orange (MO) was confirmed by decomposing the MO (10 mg/L, 500 mL) in a quartz reactor. Then, a 300 W Xe lamp was used as the light source and the suspension was continuously stirred in the dark for adsorption/desorption equilibrium. Typically, 20 mg of the photocatalyst powder was added to the MO solution and irradiated by the simulated sunlight. Then, ~5 mL of the MO solution was taken out after 20 min and the concentration was monitored by a UV-vis spectrophotometer (UV-2550) at λ = 464 nm.

3. Results and discussion

As shown in Fig. 1a, G/$Mn_{0.2}Cd_{0.8}S$ HN and G/CdS HN exhibit similar diffraction patterns. However, the diffraction peaks of G/$Mn_{0.2}Cd_{0.8}S$ HN are shifted to a higher diffraction angle due to the incorporation of small-sized Mn^{2+} ions, which leads to lattice shrinkage and indicates the formation of $Mn_{0.2}Cd_{0.8}S$ solid-solution[10]. Moreover, the graphene peaks have not been observed in both samples because (002) peak of graphene is overlapped by (100) peak of CdS[11].
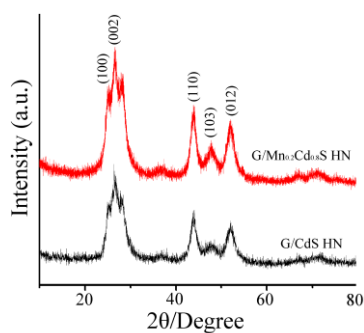
Fig. 1. XRD of the samples.
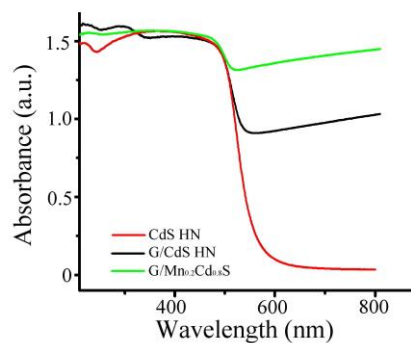
Fig. 2. UV-visible spectroscopy of the samples.
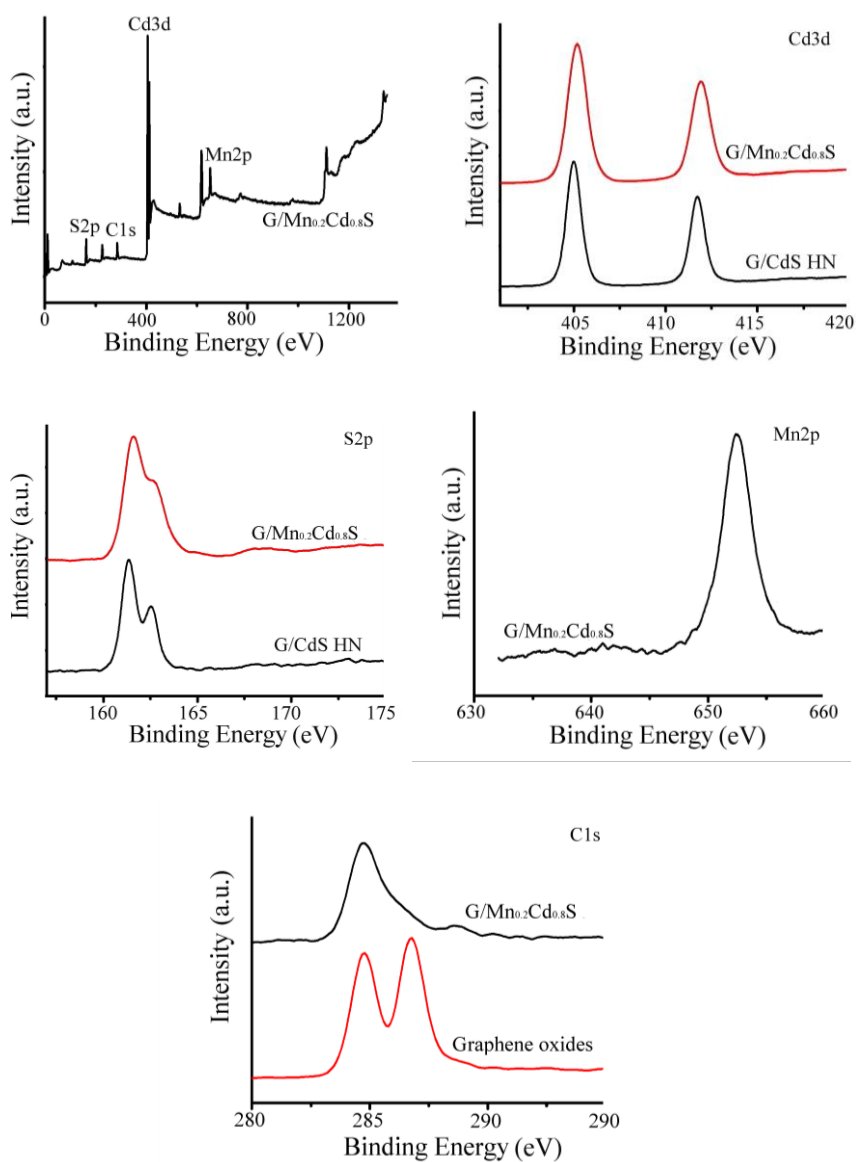
Fig. 3. Typical XPS spectra of the composite: (a) survey spectra, (b) Cd 3d region XPS spectrum, (c) S 2 p region XPS spectrum, (d) Mn2p s region XPS spectrum, (e) C1s region XPS spectrum region XPS spectrum.

The photoresponse of CdS HN, G/CdS HN, G/Mn$_{0.2}$Cd$_{0.8}$S has been evaluated by using a UV-visible spectrophotometer, as shown in Fig. 2. Compared with CdS HN, G/CdS HN exhibited a significant redshift in the visible light region due to the presence of graphene. Moreover, the addition of Mn increased the light absorption of G/Mn$_{0.2}$Cd$_{0.8}$S HN in the visible and NIR region, indicating the positive influence of both Mn-doping and graphene addition on the utilization of visible light[12]. As a result, a higher fraction of photons could be absorbed from the visible region of the solar spectrum.

The elemental composition was determined by XPS analysis. A typical wide-range XPS spectrum is presented in Fig. 3a, showing four distinct peaks at 405.08 eV, 162.08 eV, 653.08 eV, 285.08 eV, corresponding to Cd 3d, S 2p, Mn 2p and C 1s, respectively. Hence, the presence of Mn$_{0.2}$Cd$_{0.8}$S HN on graphene surface can be confirmed by XPS analysis. Fig. 3b shows high-resolution Cd 3d and S 2p spectra from G/Mn$_{0.2}$Cd$_{0.8}$S HN. The Cd 3d spectrum can be deconvoluted into Cd 3d$_{5/2}$ and Cd 3d$_{3/2}$ doublet, located at 405.18 eV and 411.88 eV, respectively. On the other hand, the S 2p spectrum can be separated into S 2p$_{3/2}$ and S 2p$_{1/2}$ peaks at 161.58 eV and 162.68 eV, respectively. Compared with the G/CdS HN, the higher binding energy of Cd and S in G/Mn$_{0.2}$Cd$_{0.8}$S HN indicated the incorporation of Mn-ions into the CdS lattice. Moreover, the peak at 652.38 eV in G/Mn$_{0.2}$Cd$_{0.8}$S HN spectrum corresponds to Mn 2p$_{1/2}$ of Mn^{2+} ions, which is similar to Mn^{2+} ions in MnS, and indicates the replacement of Cd^{2+} ions by Mn^{2+} and formation of Cd-S-Mn bond[12]. Fig. 3e presents the high-resolution C 1s spectrum from G/Mn$_{0.2}$Cd$_{0.8}$S HN sample, showing the contribution of carbon-oxygen bonds. Compared with graphene oxide (GO), the non-oxygenated aromatic sp2 carbon ring (C-C, 284.78 eV) is observed as the dominant peak and the peak intensity of oxygenated functional group of sp2 carbon (C-O, 286.78) is drastically decreased. Hence, efficient electron transportation can be realized due to the dominant sp2 carbon ring[13].

a)

b)

c)

d)
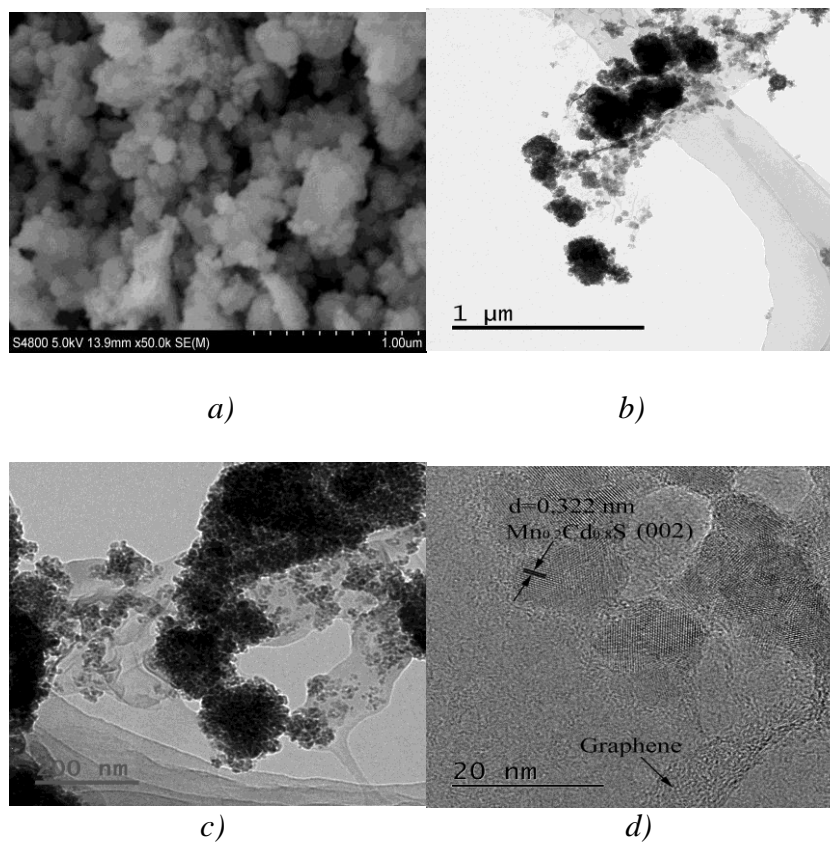
Fig. 4. (a) SEM, (b)(c) TEM, (d) HRTEM image of G/Mn$_{0.2}$Cd$_{0.8}$S.

Fig. 4 shows the typical SEM, TEM and HRTEM images of the $G/Mn_{0.2}Cd_{0.8}S$ HN samples. The field-emission scanning electron microscopy (SEM) images show the spherical morphology of $G/Mn_{0.2}Cd_{0.8}S$ HN with an average size of 50 to 100 nm and a rough surface. Fig. 4b presents typical TEM image of $G/Mn_{0.2}Cd_{0.8}S$ HN, showing a hierarchical nanostructure with uniformly anchored $Mn_{0.2}Cd_{0.8}S$ nanoparticles on graphene sheets. The high-magnification TEM image shows that the assembled nanoparticles possess spherical morphology with an average size of ~20 nm (Fig. 4c). The unique hierarchical nanostructure and abundant active nanoparticles significantly contributed to the photocatalytic properties. The high-resolution TEM image exhibits an interlayer spacing of 0.322 nm, which corresponds to (002) planes of hexagonal $Mn_{0.2}Cd_{0.8}S$ (Fig. 4d)[9].

a) *b)* *c)*

d) *e)*
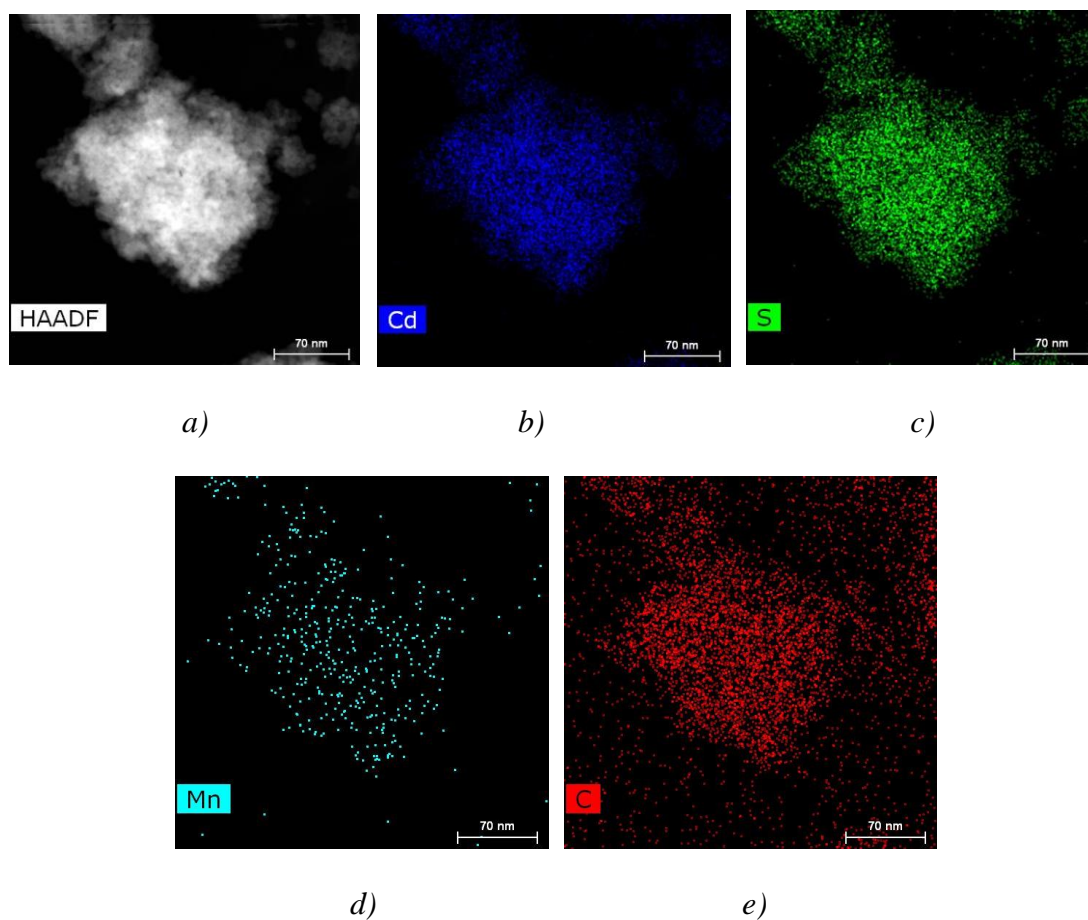
Fig. 5. (a) TEM of EDS mapping of selected area, (b) element Cd mapping,
(c) element S mapping, (d) element Mn mapping, (e) element C mapping of $G/Mn_{0.2}Cd_{0.8}S$.

Furthermore, EDS mapping was carried out to obtain further information on the structure and composition of $G/Mn_{0.2}Cd_{0.8}S$ HN hybrid. A typical SEM image shows the hierarchically arranged $Mn_{0.2}Cd_{0.8}S$ nanoparticles on graphene sheets (Fig. 5a). As shown in Fig. 5(b-d), EDS mapping confirms the presence and uniform dispersion of Cd, S, Mn elements. The uniform distribution of C can be ascribed to the graphene sheet, which acted as a substrate in $G/Mn_{0.2}Cd_{0.8}S$ HN hybrid. Hence, the proposed synthesis route results in the successful fabrication of $G/Mn_{0.2}Cd_{0.8}S$ HN and formation of $Mn_{0.2}Cd_{0.8}S$ solid-solution.
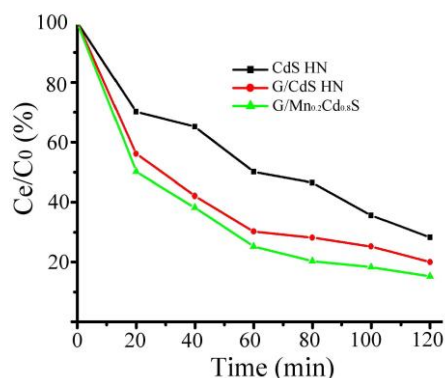
Fig. 6. Photocatalytic degradation efficiency of MO with different catalysts under visible light.

Furthermore, the photocatalytic degradation of the organic contaminants is evaluated, as shown in Fig. 6. It reveals that $G/Mn_{0.2}Cd_{0.8}S$ HN exhibited much better photocatalytic degradation efficiency for MO dye than CdS HN and G/CdS HN. The total degradation efficiency of $G/Mn_{0.2}Cd_{0.8}S$ HN reached 84.8%, whereas the degradation efficiency of CdS HN and G/CdS HN was found to be 71.7% and 80.3%, respectively. Thus, the total removal performance of $G/Mn_{0.2}Cd_{0.8}S$ HN was 1.18 times higher than CdS HN and 1.06 times higher than G/CdS HN. The superior photocatalytic activity of $G/Mn_{0.2}Cd_{0.8}S$ HN can be ascribed to (1) the hierarchical assembly of nanopheres, providing a large amount of active substance during photocatalytic reaction, (2) nano bandgap of $G/Mn_{0.2}Cd_{0.8}S$ HN (2.1-2.4 eV) and negative shift of the conduction band edge, and (3) the presence of graphene, acting as an electrons accepter and increasing the charge carrier separation.
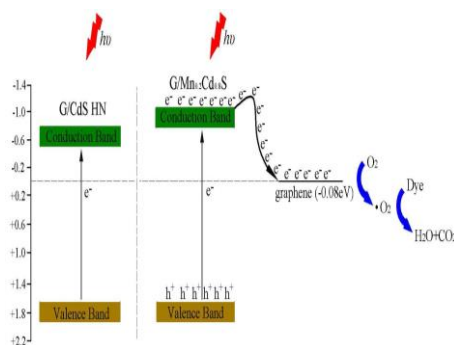
Scheme 1. Schematic illustration for the charge transfer and separation in the $G/Mn_{0.2}Cd_{0.8}S$ HN system.

The transfer of photogenerated electrons and possible photocatalytic mechanisms are illustrated in Scheme 1. First, $G/Mn_{0.2}Cd_{0.8}S$ HN is excited under the visible light irradiation and generated electron/hole pairs[14-15]. Second, owing to the infiltration of Mn^{2+} ions into CdS lattice, the CB edge has been shifted towards a more negative potential energy and promotes the photocatalytic reduction activity[10]. Third, the photogenerated electrons are rapidly transported from the conduction band of $Mn_{0.2}Cd_{0.8}S$ HN to the graphene surface due to the excellent conductivity of the graphene, realizing the efficient separation of electron/hole pairs[10]. Consequently, the dissolved oxygen acceptes the photogenerated electrons and transforms into radical peroxide anions, which could directly oxidize organic pollutants into CO_2 and H_2O[10].

4. Conclusions

In summary, G/Mn$_{0.2}$Cd$_{0.8}$S HN composites have been synthesized by using an environment-friendly Microwave-assisted hydrothermal method. The resulting G/Mn$_{0.2}$Cd$_{0.8}$S HN composites renders superior photocatalytic activity under visible light irradiation due to the hierarchical nanopheres morphology, optimal bandgap and presence of graphene scaffold, which exhibited synergistic influence on photocatalytic degradation of organic pollutants.

Acknowledgments

References

[1] X. Y. Liu, C. S. Chen. Mater. Lett. **261**, 12712766 (2020).
[2] C. S. Chen, X. Y. Liu, Q. Fang et al., Vacuum. **174**, 109108 (2020).
[3] S. S. Shenoy, E. Y. Jang, T. JooPark et al., Appl. Surf. Sci. **31**(483), 696 (2019).
[4] Q. Li, X. Li, S. Wageh, et al. Adv. Energy Mater. **5**(14), 1500010 (2015).
[5] K. Ikeue, S. Shiiba, M. Machida, Chem Sus Chem. **18**, 269 (2011).
[6] X. L. Liu, X. Z. Liang, P. Wang et al., Appl. Catal. B Environ. **203**, 282 (2017).
[7] H. L. Li, Z. Q.Wang, Y. H. He et al., J. Colloid Inter. Sci. **535**(1), 469 (2019).
[8] J. S. Lai, Y. M. Qin, L. Yu et al., Mater. Sci. in Semicon. Proc. **52**, 82 (2016).
[9] Z. H. Qun, Z. J. Tao, L. Q. Ye et al., Appl. Catal. B Environ. **237**(5), 689 (2018).
[10] B. Zeng, W. J, Zeng, J. Nanomater. Bios. **12**(1), 2015 (2017).
[11] S. Q. Liu, M. Q. Quan, J. Mater. Chem. A **2**, 430 (2014).
[12] H. Liu, Z. Z. Xu, Z. Zhang et al. Appl. Catal. A-Gen. **518**, 150 (2016).
[13] B. Zeng, X. Chen. J Nanomater. Bios. **11**(2), 559 (2016).
[14] J. M. Wang, J. Luo, D. Liu et al., Appl. Catal. B Environ. **241**, 130 (2019).
[15] X. M. Liu, B. Q. Wu, X. Y. Chen et al., Inter. J. Hydrogen Energy **45**(4), 2884 (2020).